Computer Methods in Biomechanics and Biomedical Engineering
Vol. 00, No. 00, 00 00, 1–12

Published in Computer Methods in Biomechanics and Biomedical Engineering.
Full reference: Schiller NK, Franz T, Weerasekara NS, Zilla P, Reddy BD. A simple fluid-structure coupling algorithm for the study of the anastomotic mechanics of vascular grafts. Comput Methods Biomech Biomed Eng, 2010, 13(6), 773-81.

ORIGINAL ARTICLE

A Simple Fluid-Structure Coupling Algorithm for the Study of the Anastomotic Mechanics of Vascular Grafts

N.K. Schiller[a], T. Franz[b*], N.S. Weerasekara[a], P. Zilla[b] and B.D. Reddy[a]

[a] *Centre for Research in Computational and Applied Mechanics, University of Cape Town, Rondebosch, South Africa*;
[b] *Cardiovascular Research Unit, Chris Barnard Department of Cardiothoracic Surgery, University of Cape Town, Observatory, South Africa*

(*November 2009*)

Vascular anastomoses constitute a main factor for poor graft performance due to mismatch in distensibility between host artery and graft. This work aimed at computational fluid-structure investigations of proximal and distal anastomoses of vein grafts and synthetic grafts. Finite element and finite volume models were developed and coupled by a user-defined algorithm. Emphasis was placed on simplicity of the coupling algorithm. Artery and vein graft showed a larger dilation mismatch than artery and synthetic graft. The vein graft distended nearly double compared to the artery while the synthetic graft displaying only approximately half the arterial dilation. For the vein graft, luminal mismatching was aggravated by development of an anastomotic pseudo-stenosis. While this study focused on end-to-end anastomoses as a vehicle for developing the coupling algorithm, it may serve as useful point of departure for further investigations such as other anastomotic configurations, refined modelling of sutures, and fully transient behaviour.

Keywords: Anastomosis; Vascular graft; Artery; Blood vessel; Blood flow; Computational fluid dynamics; Finite element method

1. Introduction

Atherosclerosis, the hardening and narrowing of arteries, is the most common type of arterial disease (Noble et al. 2005) which is accountable, directly or indirectly, for about half the deaths in the western world. This and other forms of coronary and peripheral vascular diseases are treated by surgical intervention. Bypass grafting uses autologous conduits, such as internal mammary artery and saphenous vein, and synthetic grafts, typically expanded polytetrafluorethylene (ePTFE) or poly(ehtylene terephthalate) (Dacron) (Tiwari et al. 2003). One of the most prominent reasons for poor performance and failure of small and medium sized grafts is the development of anastomotic intimal hyperplasia (AIH), in particular at the distal anastomosis. The causes of AIH range from surgical trauma and lack of endothelium to compliance mismatch and disturbed flow conditions. It is believed that flow conditions and shear stress are the most dominant factors for hyperplastic response (Zilla et al. 2007).

The anastomotic configuration and compliance mismatch not only depend on the mechanical properties of host vessel and graft, but also on suture material

*Corresponding author. Email: thomas.franz@uct.ac.za

ISSN: 1741-5977 print/ISSN 1741-5985 online

DOI: 10.1080/1741597YYxxxxxxxx
http://www.informaworld.com

and suturing technique. Mechanics and compliance mismatch of end-to-side and end-to-end anastomoses have received extensive attention in in-vivo, in-vitro, and numerical studies (Tiwari et al. 2003; Migliavacca and Dubini 2005). Computational approaches have been used to evaluate fluid and structural quantities such as fluid shear stress and circumferential wall stress and strain which are rather difficult to measure in-vivo. The optimization of the anastomotic configuration with regard to fluid and structural mechanics has been a major target of computational studies (Migliavacca and Dubini 2005).

This study investigated, by means of a simple approach, the effects of compliance mismatch between host vessel and vascular graft and suturing techniques on the structural and fluid mechanics of proximal and distal end-to-end anastomoses. The study combined computational solid mechanics, fluid mechanics, and fluid-structure interaction. Anastomotic parameters included three vascular materials (arterial and venous soft tissue, and porous polyurethane) and the interrupted suturing technique. The vascular soft tissue was modelled as a two-layer isotropic, hyperelastic material and the porous polymer as a hyperfoam material. In order to carry out an axisymmetric simulations, the effect of the sutures was modelled by a smeared-out, orthotropic linear elastic material which was uniformly distributed around the circumference. The blood was assumed to be a Newtonian fluid, with flow being pulsatile and turbulent.

2. Methods

To simulate the phenomenon being studied in both the solid and the fluid problem, the following commercial software packages were used: *Abaqus*® for the finite element solid modelling, *Gambit*® for the mesh generation of the fluid domain, and *Fluent*® to simulate the fluid flow.

2.1 Solid Modelling

2.1.1 Strain Energy Function for Vascular Soft Tissue

In order to represent the hyperviscoelastic properties of the artery as realistically as possible, a strain energy function was needed (Holzapfel et al. 2000; Delfino et al. 1997). Hyperelasticity was deemed an acceptable approximation as the simulations in this work considered loading conditions within the normal physiological range. Delfino et al. (1997) proposed a strain-energy function, with an isotropic rubber-like strain-energy potential, to model the behaviour of a carotid artery under loading. This strain energy function was used here to define the hyperelastic properties of arterial and venous soft tissue. The function is given by

$$U = \frac{a}{b}\left\{\exp\left[\frac{b}{2}\left(I_1 - 3\right)\right] - 1\right\} \tag{1}$$

where a and b are material parameters. With this strain-energy function it was possible to achieve the typical response in the high pressure region. Material incompressibility was assumed, hence $I_3 = 1$. The constants used to model the arterial and venous soft tissue sections, mimicking the artery and vein-graft (Delfino et al. 1997; Koch et al. 2009) are given in Table 1. A UHYPER function adapted from previous work (Delfino et al. 1997; Koch et al. 2009; Schaefer 2006), was used to implement these models in *Abaqus*®.

Table 1. Strain Energy Constants for Adventitial and Medial Layer of Artery and Vein

	Artery_{Adv}	Artery_{Med}	Vein_{Adv}	Vein_{Med}
a (Pa)	27370	44200	20000	27370
b	4.74	8.35	2.50	4.71

2.1.2 Hyperfoam for Synthetic Graft Material

The synthetic graft was based on a porous polyurethane structure produced by methods described by Bezuidenhout et al. (2002). The hyperelastic graft material was modelled using a hyperfoam model with a strain-energy function described by Yeoman et al. (2009), Storkers (1986) and Odgen (1984):

$$\begin{aligned} U &= U(\bar{\lambda}_1, \bar{\lambda}_2, \bar{\lambda}_3) \\ &= \sum_{i=1}^{n} \frac{2\mu_i}{\alpha_i^2} \left[\left(\bar{\lambda}_1^{\alpha_i} + \bar{\lambda}_2^{\alpha_i} + \bar{\lambda}_3^{\alpha_i} - 3 \right) + 3 \left(J_{el}^{\frac{1}{3}\alpha_i} - 1 \right) + \frac{1}{\beta_i} \left(J_{el}^{-\alpha_i \beta_i} - 1 \right) \right] \end{aligned} \tag{2}$$

where λ_i are the principal stretches, $\bar{\lambda}_i = J^{-\frac{1}{3}} \lambda_i$, J_{el} is the elastic volume strain and μ_i, α_i and β_i are temperature dependent material parameters. If all β_i are equal to a constant value β, one can define the effective Poisson's ratio

$$\nu = \frac{\beta}{1 + 2\beta}. \tag{3}$$

The hyperfoam coefficients for the porous polymer in *Abaqus*® are given in Table 2 and correspond to the material with porogen size of 90-106μm investigated by Yeoman et al. (2009).

Table 2. Hyperfoam model coefficients for synthetic graft

ν	0.08
μ_1	0.5411×10^6
μ_2	-0.1528×10^6
μ_3	-0.3936×10^6
μ_4	0.1337×10^6
α_1	2.449
α_2	4.694
α_3	-1.575
α_4	-3.571

2.1.3 Orthotropic Material for Anastomotic Interface

A 2D axisymmetric model was used to simulate the presence of the sutures. The suture properties were incorporated in an averaging fashion by replacing the discrete sutures with a continuous band of material with properties that exhibit the overall effect of the sutures. As the suture had a much higher stiffness in comparison to the vascular soft tissue and synthetic graft sections, this behaviour was modelled by treating the band as an orthotropic material which was much stiffer in the axial than in the radial direction.

As the deformations in the suture were expected to be small, small-strain elastic theory was employed. In order to simulate the *Prolene*® suture, based on a previous study (Aguirre et al. 2003) a Young's modulus of 18.53 MPa was used. The 12 stitches with two segments each typically found in an anastomosis with a 4 mm diameter were approximated to a smear to be modelled in a 2D axisymmetric model. Based on the volumetric composition a volumetric average value of 0.969

MPa for the Young's modulus was computed in the axial direction while the radial direction value was considered to be 10% of the computed value. The value of Poisson's ratio ν was set at 0.49.

2.1.4 Finite Element Models

The anastomotic wall region was subdivided into different partitions, as shown in the section through the walls in Fig. 1. A small partition consisting of two rows of elements at the region of the anastomosis was defined as the suture smear. The remaining divisions of the model, were those of the artery and graft, where an arterial section was divided again longitudinally to create two equally thick layers representing the media and adventitia. A further partition was created for the graft; in the case of the vein graft the same procedure as that for the artery section was followed.

Inner and outer diameters of 4 and 5 mm were used respectively for the anastomotic model. Schajer et al. (1996) suggested a length of twice the diameter in modelling anastomosis computationally, thus a 10 mm section was chosen for both the artery and the graft, and 0.2 mm for the suture smear was used.

Four-noded bilinear hybrid elements with constant pressure were used in axisymmetric analyses. The mesh generated for this model corresponded to that of the fluid domain as the common boundary nodes had to be in the same geometric location. A mesh of 200 elements in the axial direction and 8 elements in the radial direction was chosen. This resulted in 1600 elements defined by 1809 nodes. The inputs loading for the models are given in Table 3 (Delfino et al. 1997; Zhang et al. 2007).

Table 3. 2D Axisymmetric Model Inputs

Input	Value
Longitudinal Prestress	10 % of section length
External Pressure	8.6 kPa (65 $mmHg$)
Luminal Pressure	$10.6 - 16.0$ kPa $(80 - 120$ $mmHg)$

2.2 Fluid Flow Modelling

Blood was modeled as an incompressible, isothermal, Newtonian fluid. Though some researchers (O'Callaghan et al. 2006) have shown blood may behave as a non-Newtonian fluid due to the shear rates present in human arteries, for simplicity Newtonian behavior was assumed. For incompressible fluids the equation of mass conservation becomes the continuity equation

$$\operatorname{div} \mathbf{v} = \mathbf{0} \tag{4}$$

where $\mathbf{v}$ is the velocity field. Neglecting body forces, the equation for conservation of momentum for incompressible Newtonian fluids is given by

$$\rho \frac{\partial \mathbf{v}}{\partial t} + \rho(\mathbf{v} \cdot \nabla)\mathbf{v} = -\nabla p + \mu \nabla^2 \mathbf{v} + \mathbf{V} \tag{5}$$

where ρ is the mass density, μ is the dynamic viscosity, p is the pressure and $\mathbf{V}$ represents terms arising from the additional viscous stress (Patankar 1980).

The pulsatile blood flow was assumed to be in a transitional region and the low Reynolds number $k - \omega$ turbulence model was used (Li et al. 2007). Here k is the

turbulent kinetic energy and ω is the specific dissipation rate. These variables must satisfy the following two transport equations:

$$\frac{\partial}{\partial t}(\rho k) + \text{div}\ (\rho k \mathbf{v}) = \text{div}\ (\Gamma_k \nabla k) + G_k - Y_k + S_k\,, \tag{6}$$

$$\frac{\partial}{\partial t}(\rho \omega) + \text{div}\ (\rho \omega \mathbf{v}) = \text{div}\,(\Gamma_\omega \nabla \omega) + G_\omega - Y_\omega + S_\omega\,. \tag{7}$$

where G_k and G_ω represent the generation of turbulence kinetic energy and of ω due to mean velocity gradients. The effective diffusivity is represented by Γ_k and Γ_ω, dissipation due to turbulence is represented by Y_k and Y_ω and lastly the source terms are represented by S_k and S_ω (Ansys 2005).

The flow modelling was carried out using the PISO velocity-pressure coupling algorithm, with the k - ω turbulence model, discretisation schemes of standard pressure as well as second order upwind for momentum, turbulence kinetic energy and specific dissipation rate were used. A mesh with 40 elements in the radial and 200 elements in the axial direction was created using *Gambit*®, where a length of 20 mm and a radial width of 2 mm was considered for the flow domain, with the 200 elements in the axial direction corresponding to the 200 elements of the solid model. A boundary layer consisting of 10 elements from the arterial wall was implemented to create a finer mesh in this region. In addition, boundary conditions were assigned to the flow domain. These included velocity inlet, pressure outlet, symmetry axis and wall boundary. The inlet flow velocity profile during a cardiac cycle was represented by approximating the velocity inflow wave form in Fig. 2, valid for arteries with an internal diameter of $4mm$ (Politis et al. 2008), with a cubic spline function.

2.3 Fluid-Structure Interaction Model

The nature of the problem described was defined by two systems. It was thus essential to study the coupled behaviour of the blood flow and the structural region of anastomosis. This process was broken down into the following steps:

(a) Simulation of the blood flow, using CFD, resulting in a pressure profile at the arterial wall;
(b) Analysis of the artery-graft model, using FEM, with the pressure profile obtained in step (a) as loading condition, providing the displacements of the solid artery–graft model corresponding to the pressure loading;
(c) Adaptation of the fluid domain using the displacements from step (b), and repeat of the fluid flow simulation;
(d) Continuation of the iterative process until variation in geometry at every nodal point falls below a prescribed tolerance for convergence defined as:

$$\frac{d^{i+1} - d^i}{d^i} \leq 1 \times 10^{-4} \tag{8}$$

where d^i is the nodal displacement in the i^{th} iteration of the arterial–graft anastomosis wall.

This algorithm is illustrated in Fig. 3.

The meshes of solid and fluid domain coincided along the common boundary throughout the iterative analysis including adaptation of domain geometries. A bespoke grid adaptation algorithm was employed for adjustment of nodal coordinates of the fluid domain. This ensured that fine mesh details were maintained during geometric adaptation of the fluid domain. New nodal coordinates for the common wall boundary nodes were accommodated in the fluid domain by interpolative adjustment of the radial coordinates of internal nodes while axial coordinates of the nodes were kept unchanged. The interpolation of the radial coordinates was performed with the following equation:

$$\frac{y_{2,i+1} - y_{1,i+1}}{y_{b,i+1} - y_{a,i+1}} = \frac{y_{2,i} - y_{1,i}}{y_{b,i} - y_{a,i}} \tag{9}$$

where the subscripts i and $i+1$ refer to the initial and the new grid values, the subscripts 1 and 2 denote neighbouring nodes, and subscripts a and b refer to the corresponding nodes on axis and wall boundary, respectively.

3. Results

3.1 Vein Graft Proximal Anastomosis (Blood Flow from Artery to Vein Graft)

The vein graft dilated more than the arterial region after the longitudinal prestress, external and luminal pressures were applied, see Fig. 4a-c for an operating pressure of 13.3 kPa. The anastomotic interface with the suture behaved less compliantly than both the artery and the vein graft thereby forming a pseudo-stenosis. The inner diameter of the artery and the vein graft increased to 4.5 mm and 4.95 mm, while dilation of the anastomotic interface was limited to 4.06 mm internal diameter. The wall thickness of artery and vein decreased from 0.5 mm in the unloaded state to 0.42 and 0.38 mm, respectively, at 13.3 kPa pressure. This constituted a wall thinning of 16.0% and 24.0% in artery and vein, see Table 4.

Figure 5a illustrates the absolute pressure of the fluid domain, i.e. the luminal blood pressure in artery and vein graft. The absolute pressure was obtained as the pressure field, in addition to the operating pressure of 13.3 kPa, once interaction was established between the deformation of the artery, vein graft and the blood flow. A slight pressure drop was observed at the anastomotic interface. The flow entered a converging region just proximal to the anastomosis, causing an increase in velocity (see Fig. 4a) and a decrease in pressure. As the vein graft dilated distally to the anastomosis, the velocity dropped and the pressure rose slightly due to the diffusing effect of the diverging profile. The maximum and minimum pressure remained in the physiological pressure range experienced during a cardiac cycle.

The change in absolute pressure during one cardiac cycle is illustrated in Fig. 5a. The curve for t = 0.2 s corresponds to the velocity at peak systole (Fig. 2). At this point the blood flow velocity was maximum, the lowest pressure during a cardiac cycle was thus expected. The converse was shown for the maximum pressure, recorded at the lowest velocities during the cardiac cycle, from 0 - 0.1 s and again between 0.7 - 1.0 s. The low velocity at the end of the cardiac cycle allowed for a high pressure.

The maximum principal stresses in the media and adventitia were 35 kPa and 10 kPa, respectively, for the artery and 48 kPa and 19 kPa for the vein (see also Fig. 4b). These differences reflected the variation in material properties between

the tissue types (arterial vs. venous) and tissue layers (media vs. adventitia). A stress concentration with a value of 62 kPa was observed at the low-compliance anastomotic interface with the suture line.

3.2 Vein Graft Distal Anastomosis (Blood Flow from Vein Graft to Artery)

As in the proximal case, the vein graft was more compliant than the artery, which was confirmed by the results shown in Fig. 4d-f. The pressure drop across the anastomosis was again observed (Fig. 5b), for the same reasons as in the proximal model. It is interesting to note that the absolute pressure was higher throughout the entire anastomotic region for distal case compared to the proximal case (Fig. 5a). This was attributed to the larger distension of the 'inlet' region, formed by the vein graft, in the distal configuration compared to the proximal configuration where the artery represented the 'inlet'.

The distended diameter of the three different vascular regions, namely vein graft, artery, and anastomotic interface, was 4.96 mm, 4.5 mm and 4.06 mm, respectively, which closely matched the values observed in the proximal case. The slight stenosis formed at the anastomotic interface indicated again the effect of the suture. The change in diameter from the larger vein graft to the smaller artery resulted in an increase in pressure at the centre of the lumen. Due to the sharp dent at the anastomosis, low pressures were recorded along the arterial wall. A similar phenomenon was observed in the velocity profile, where the velocity at the centre of the lumen was high, but decreased quickly with respect to radius.

The wall thinning in both sections agreed with the values observed in the proximal configuration, namely 16.0% in the artery and 24.0% in the vein.

The adventitia and the media layer could be clearly distinguished with respect to maximum principal stress in both vascular sections, see Fig. 4e. The maximum stress was 39 kPa and 30 kPa in the media of vein graft and artery, and 12 kPa and 10 kPa in the adventitia of vein graft and artery.

3.3 Synthetic Graft Proximal Anastomosis (Blood Flow from Artery to Synthetic Graft)

In this case, the artery dilated more (internal diameter 4.0 mm to 4.41 mm) than the synthetic graft (4.0 mm to 4.22 mm). The magnitude of the diameter mismatch of the distended artery and synthetic graft was smaller (4.5%) than in the artery to vein graft case (10.0%), resulting in smaller changes of the flow domain (Fig. 6a and c). In addition, the anastomotic interface did not form a stenosis as it distended to 4.24 mm, closely matching the distended graft diameter. The lower diameter mismatch and, more importantly, the absence of an anastomotic stenosis resulted in a flow domain with nearly constant cross-sectional dimension. This led to a negligible pressure change across the anastomosis, as opposed to the distinct pressure drop observed in the artery - vein graft case (compare Fig. 5c and a), and the lack of a notable change in the velocity profiles across the anastomotic interface (Fig. 6a).

Differences between arterial and synthetic graft section were also observed in wall thinning. The thickness of the arterial wall, consisting of media and adventitia, was reduced by 18.0% to 0.41 mm which agreed with the value observed in the artery-vein case. A considerably lower wall thinning of 5.0% (wall thickness: 0.5 to 0.48 mm) was however predicted for the synthetic graft.

The media and adventitia of the artery exhibited maximum principal stress values of 38 kPa and 12 kPa, respectively, which were 8.6% and 20.0% higher than those

predicted for the proximal artery-vein case. The maximum principal stress in the synthetic graft wall was predicted to 18 kPa. The distribution of the maximum principal stress is illustrated in Fig. 6b.

3.4 Synthetic Graft Distal Anastomosis (Blood Flow from Synthetic Graft to Artery)

The pressurized synthetic graft – artery model (Fig. 6e and f) indicated that the artery dilates slightly more (4.42 mm) than the synthetic graft (4.23 mm) and the anastomotic interface (4.25 mm), similar to the proximal configuration. The wall thinning in artery and graft was 18.0% and 5.0%, respectively, as predicted for the proximal configuration.

The maximum principal stresses in this configuration are illustrated in Fig. 6e. The media and adventitia of the artery exhibited values of 36 kPa and 11 kPa, respectively, compared to 17 kPa in synthetic graft wall. These values were slightly lower than the respective maximum principal stresses observed in the proximal case. This was attributed to a lower pressure which resulted, due to energy conservation, from a smaller inlet diameter (synthetic graft: 4.23 mm) compared to the proximal case (artery: 4.42 mm) in combination with the same inlet velocity. The flow did not show discontinuities across the anastomotic interface, Fig. 6d, and remained similar to the proximal case (Fig. 6a).

Table 4. Predicted results for various sections of anastomotic models (A: Artery, An: Anastomosis, VG: Vein graft, SG: Synthetic graft): Minimum and maximum internal diameter (D_{min}, D_{max}), Change in internal diameter (ΔD), Maximum stress in Media ($\sigma_{max,Med}$) and Adventitia ($\sigma_{max,Adv}$), Wall thickness at p = 0 kPa ($t_{w,p=0}$) and at p = 133 kPa ($t_{w,p=133}$)

	Artery – Vein Graft						Artery – Synthetic Graft					
	Proximal			Distal			Proximal			Distal		
	A	An	VG	A	An	VG	A	An	SG	A	An	SG
D_{min} $[mm]$	4.00	4.00	4.00	4.00	4.00	4.00	4.00	4.00	4.00	4.00	4.00	4.00
D_{max} $[mm]$	4.50	4.06	4.95	4.50	4.06	4.96	4.41	4.24	4.22	4.42	4.25	4.25
ΔD [%]	12.5	1.5	23.8	12.5	1.5	24.0	10.3	6.0	5.5	10.5	6.3	5.8
$\sigma_{max,Med}$ $[kPa]$	35		48	30		39	38		18	36		17
$\sigma_{max,Adv}$ $[kPa]$	10		19	10		12	12		18	11		17
$t_{w,p=0}$ $[mm]$	.50		.50	.50		.50	.50		.50	.50		.50
$t_{w,p=max}$ $[mm]$	.42		.38	.42		.38	.41		.48	.41		.48
Δt_w [%]	16.0		24.0	16.0		24.0	18.0		5.0	18.0		5.0

4. Discussion

The objective of this work was to study the mechanical behaviour of peri-anastomotic vascular regions using computational techniques, with a particular goal being the development and implementation of a simple algorithm to account for fluid-structure interaction. The algorithm made full use of specialised solid and fluid mechanics-based commercial packages, and its key feature lies in a simple iterative procedure for achieving the coupling.

The developed and implemented algorithm, though simple in structure, was an effective means for exploring anastomotic behaviour in a fully coupled context. In particular, it permitted a detailed computational exploration of the behaviour of anastomoses for vein- and synthetic grafts with arteries.

The artery-vein graft anastomoses displayed considerable mismatch of the mechanical behaviour with the diameter increase of the vein graft upon exposure to arterial mean blood pressure being nearly double that of the artery. The synthetic graft behaved far stiffer than the vein graft, here the graft dilation was about 50 % of the arterial dilation. In all cases, the predicted diameter mismatch indicates changes of the physiological flow domain and arterial circulation which is further aggrevated by the low-compliant anastomotic interface (suture line). Interestingly, the dilation of the anastomosis, though modeled identically in all cases, showed counterintiuitve pattern: a larger dilation was predicted in the stiffer peri-anastomotic configurations of artery-synthetic graft compared to the more distensible artery-vein graft models.

The results show a larger dissimilarity of maximum principal stresses and wall thinning between proximal and distal anastomoses for the artery-vein case compared to the artery-synthetic graft case. This difference was attributed to the larger discrepancy in mechanical properties between artery and vein leading to a more discontinuous flow domain compared to the artery-synthetic graft models. A notable difference is observed between the distended diameter of the anastomotic interface for artery-vein model and the artery-synthetic graft model. In combination with larger dilations in the artery-vein model, the anastomotic interface had a stenotic effect, adding to structural and flow discontinuities which found expression in a considerable anastomotic pressure drop that was not observed for the artery-synthetic graft in absence of an anastomotic stenosis.

The difference in dilation of the anastomotic interface in the models of artery-vein graft and artery-synthetic graft warrants further investigation. Although the suture and anastomotic technique were represented identically, the dilation of the artery-vein interface was merely 25% of the dilation observed in the artery-synthetic graft case. This is particularly surprising since the smaller anastomotic dilation is observed in connection with larger dilation of the graft.

Review of the values of wall thinning of all four models indicated an association with the distension of the blood vessel: Increased vessel distension generally led to increased wall thinning. Wall thinning was constituted by (transverse) wall contraction associated with the circumferential wall stretch, and wall compression due to pressure loading. Considering that all models were analysed at the same operating pressure (13.3 kPa), wall contractions seemed, however, to play a dominant role in the wall thinning process.

The distribution of maximum principal stress in media and adventitia in the arterial sections was fairly similar in all models; maximum adventitial stress levels reached between 29 and 33% of the stress in the media. Similarly, for the venous sections the stress in the adventitia reached 31% of that in the media in the distal configuration whereas it increased to 40% of the medial stress in the proximal anastomosis. The vein in the proximal anastomosis was the section displaying highest stress levels overall, exceeding stresses in venous media and adventitia in the distal anastomosis by 23 and 58%, respectively, although the distended inner vein diameter was nearly the same for proximal (4.95 mm) and distal anastomosis (4.96 mm). The difference in medial and adventitial stresses of vein and artery (the latter serves as reference) were 90 and 37% in the proximal configuration and 30 and 20% in the distal anastomosis. For the synthetic graft, the maximum principal wall stress, in absence of different layers, differed from the stress in arterial media and adventitia by -53 and 50% for the proximal configuration and -53 and 55% for the distal configuration.

Proximal and distal anastomoses were modeled individually by applying the same loading conditions to the inlet boundary which was the artery for the proximal

anastomosis and the graft (vein and synthetic, respectively) for the distal anastomosis. The scope of an extended investigation may be to represent the graft as a continuous model extending from proximal to distal anastomosis or to apply the geometric and flow conditions of the outlet of the proximal anastomosis as inlet conditions for the distal anastomosis.

5. Conclusion

The anastomotic behaviour was reviewed by examining the effects of the suturing and graft material on mismatch in dilation of the host vessel and the graft. In addition, blood flow models were generated to simulate the flow of blood in arteries and grafts, resulting in a better understanding of the properties of this flow phenomenon.

The artery-vein graft anastomoses showed a definitive dilation mismatch, where the vein graft distended to a greater extent than the artery, as observed in clinical practice. Here, constrictive external reinforcement of the vein graft will be beneficial to match dilation and flow domains of vein graft and host artery. While the artery-synthetic graft peri-anastomotic region showed a lower mismatch in dilation then the artery-vein graft case, the sub-arterial compliance of the synthetic graft bears problems of different nature, such as longterm patho-physiological changes.

This study focused on simple end-to-end anastomoses as a vehicle for developing the algorithm. These initial investigation serve as a useful point of departure for various extensions: for example, other anastomotic configurations, more refined modelling of sutures, and fully transient behaviour. A particular feature that merits further investigation is that of the counter-intuitive behaviour of the anastomotic interface, with the larger dilation observed in the less compliant artery-synthetic graft.

Conflict of Interest Statement

The authors confirm that they do not have conflicts of interests in connection with the manuscript submitted and the work and data presented therein.

References

Aguirre A, Oliva M, Schoephoerster R, Kasyanov V. 2003. Static and Dynamic Mechanical Testing of a Polymer with Potential use as Heart Valve MaterialIn: *Summer Bioengineering Conference, June 25-29, Key Biscayne, FL, USA*. June.

Ansys. *Fluent User Manual*. 2005.

Bezuidenhout D, Davies N, Zilla P. 2002. Effect of well defined dodecahedral porosity on inflammation and angiogenesis. ASAIO J 48:465–71.

Delfino A, Stergiopulos N, Moore J, Meister J. 1997. Residual Strain Effects on the Stress Field in a Thick Wall Finite Element Model of the Human Carotid Bifurcation. J. Biomechanics 30:777–786.

Holzapfel G, Gasser T, Ogden R. 2000. A new constitutive framework for arterial wall mechanics and a comparative study of material models. Computational Biomechanics 61:1–48.

Koch TM, Reddy BD, Zilla P, Franz T. 2009. Aortic valve leaflet mechanical properties facilitate diastolic valve function.. Computer Methods in Biomechanics and Biomedical Engineering ePub, DOI 10.1080/10255840903120160.

Li M, Beech-Brandt J, John L, Hoskins P, Easson W. 2007. Numerical analysis of pulsatile blood flow and vessel wall mechanics in different degrees of stenoses. Journal for Biomechanics 40:3715–3724.

Migliavacca F, Dubini G. 2005. Computational modeling of vascular anastomoses. Biomechan Model Mechanobiol 3:235–250.

Noble A, Johnson R, Thomas A, Bass P. 2005. The Cardiovascular System. 1st ed. ed. Elsevier Churchill Livingstone.

O'Callaghan S, Walsch M, McGloughlin T. 2006. Numerical modelling of Newtonian and non-Newtonian representation of blood in distal end-to-side vascular bypass graft anastomosis. Medical Engineering and Physics 28:70–74.

Odgen R. 1984. Non-linear elastic deformations.. Wiley and Sons.

Patankar S. 1980. Numerical heat transfer and fluid flow. New York, London: Hemisphere Publishing.

Politis A, Stavropoulosb G, Christolisa M, Panagopoulosb P, Vlachosc N, Markatos N. 2008. Numerical modelling of simulated blood flow in idealized composite arterial coronary grafts: Transient flow. Journal of Biomechanics 41:25–39.

Schaefer M. 2006. Numerical Investigation of the Mechanical Behaviour of Anastomotic Regions in Vascular GraftsBSc thesis, University of Cape Town.

Schajer G, Green S, Davis A, Hsiang Y. 1996. Influence of Elastic Nonlinearity on Arterial Anastomotic Compliance. Journal for Biomedical Engineering 118:445–451.

Storkers B. 1986. On material representation and constitutive branching in finite compressible elasticity. Journal of the Mechanics and Physics of Solids 34(2):125–145.

Tiwari A, Cheng K, Salacinski H, Hamilton G, Seifalian A. 2003. Improving the Patency of Vascular Bypass Grafts: the Role of Suture Materials and Surgical Techniques on Reducing Anastomotic Compliance Mismatch. Eur J Vasc Endovasc Surg 25:287–295.

Yeoman MS, Reddy BD, Bowles HC, Zilla P, Bezuidenhout D, Franz T. 2009. The use of finite element methods and genetic algorithms in search of an optimal fabric reinforced porous graft system.. Ann Biomed Eng 37(11):2266–2287.

Zhang W, Liu Y, Kassab G. 2007. Flow-induced shear strain in intima of procine coronary arteries. Journal of Applied Physiology 103:587–593.

Zilla P, Bezuidenhout D, Human P. 2007. Prosthetic vascular grafts: Wrong models, wrong questions and no healing. Biomaterials 28:5009–27.

Figures

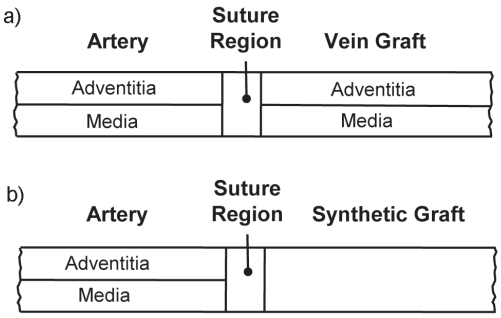

Figure 1. 2D axisymmetric partitioning of peri-anastomotic vascular wall.

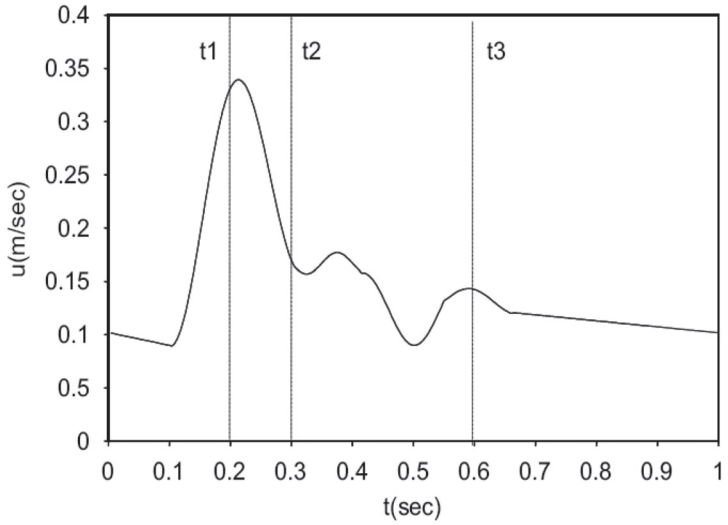

Figure 2. Inlet flow velocity profile ($\phi_{internal} = 4mm$). (Politis et al. 2008)

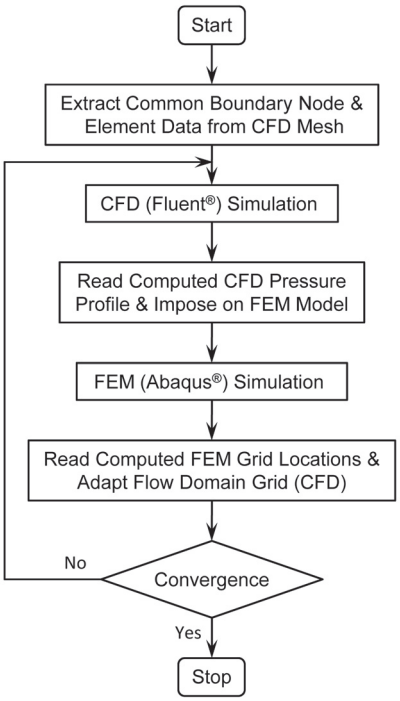

Figure 3. Sequence of the coupled simulation.

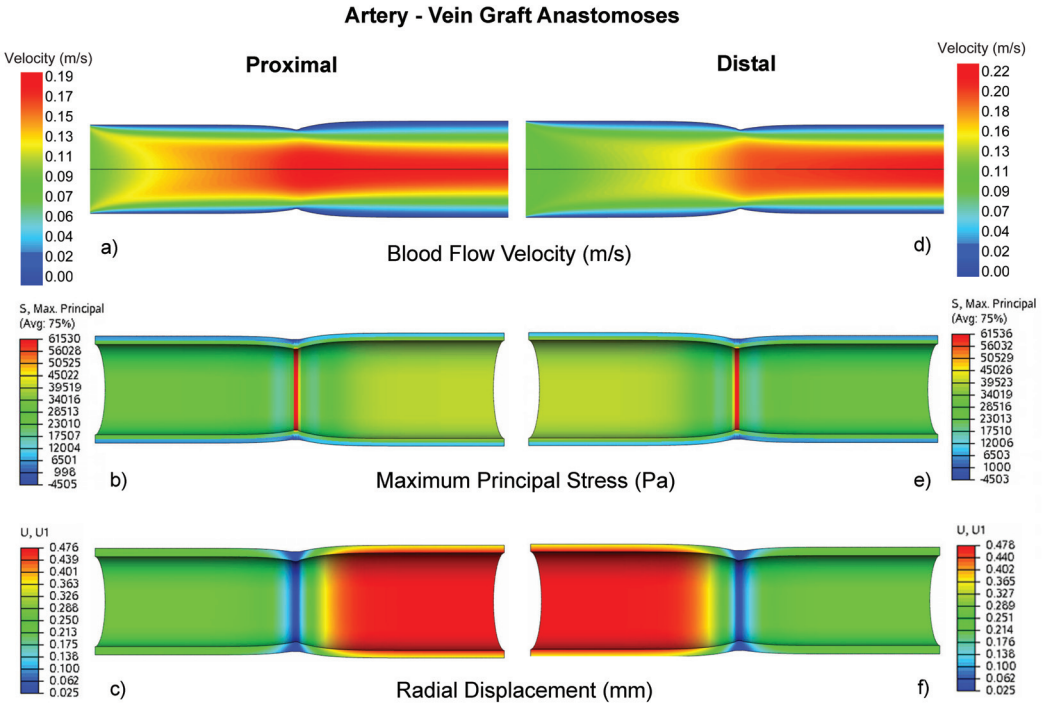

Figure 4. Predicted blood flow profiles and flow induced stress in artery to vein graft anastomosis. Note: Blood flow from left to right.

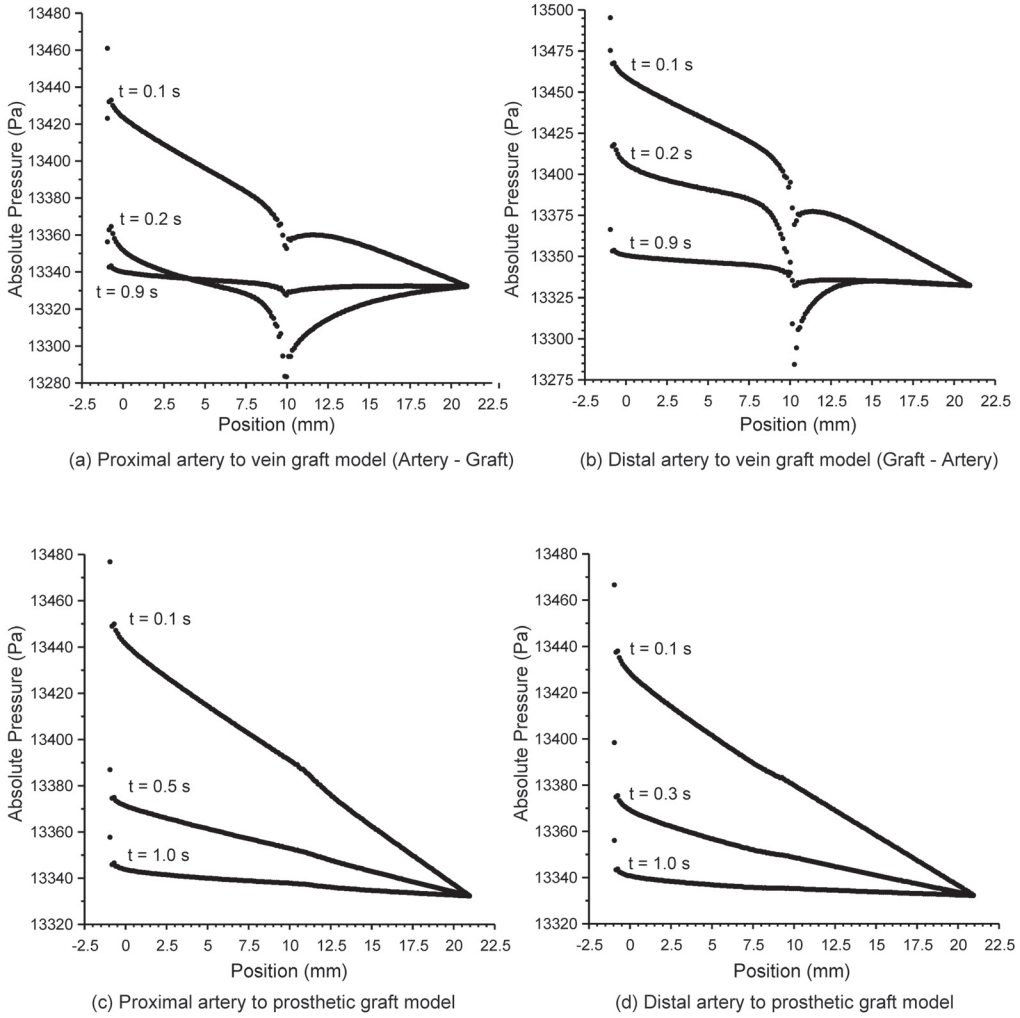

Figure 5. Plots showing the absolute pressure along the anastomosis wall at different times during the cardiac cycle.

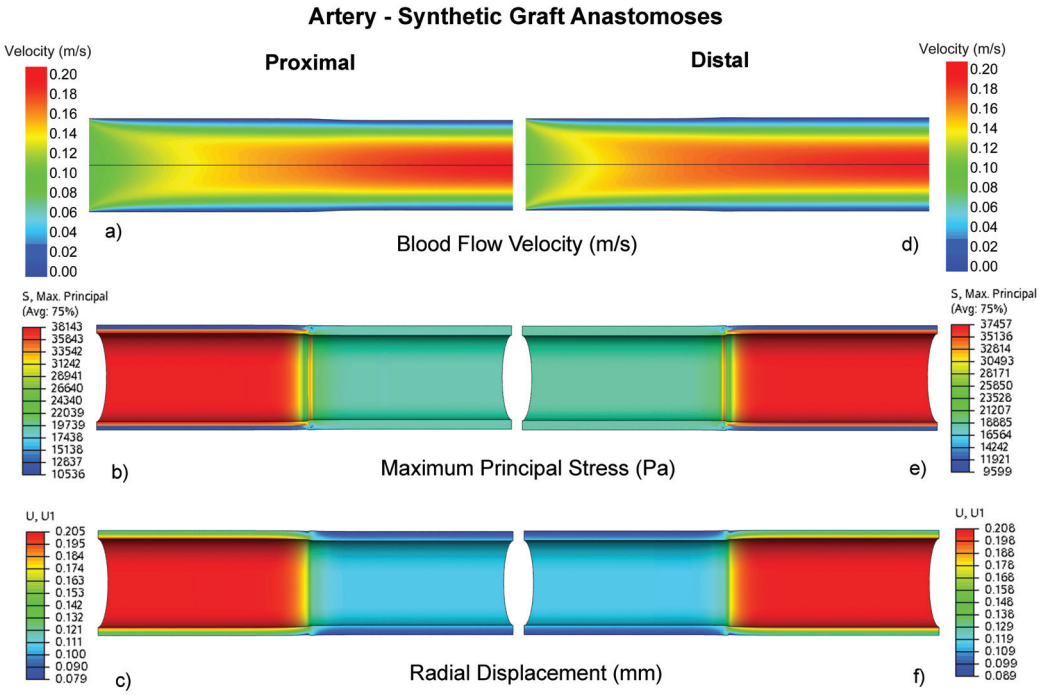

Figure 6. Predicted blood flow profiles and flow induced stress in artery to synthetic graft anastomosis. Note: Blood flow from left to right.